On the Optimality of Spectrally Notched Radar Waveform & Filter Designs

Jonathan W. Owen, Patrick M. McCormick, Christian C. Jones, Shannon D. Blunt
Radar Systems Lab (RSL), University of Kansas, Lawrence, KS

Abstract—**Designing radar waveforms with notched spectral regions can mitigate mutual interference with other proximate RF users. However, this capability comes at the cost of degraded range-Doppler sidelobe performance. To evaluate the limitations of correlation-based processing, the null-constrained power spectral density that minimizes correlation sidelobe levels is determined for comparison with waveform and pulse compression filter design methods. Existence of the least-squares (LS) global optimum indicates a fundamental dynamic range limitation for notched power spectra (notwithstanding further receive compensation or range resolution spoiling).**

Recent work investigated spectrally notched random FM (RFM) waveform design where ad-hoc tapering was incorporated into the null shape as a heuristic means of reducing range sidelobes. Here, waveforms designed according to the optimal null-constrained spectral template are demonstrated to have improved sidelobe performance after pulse compression and slow-time processing. Further, because these waveforms are designed according to the LS optimal spectral template, application of the LS mismatched filter provides additional sidelobe reduction (toward the global limit) with minimal mismatch loss.

Keywords—cognitive radar, waveform diversity, spectrum sharing

I. Introduction

The pace of increasing spectral congestion creates a major challenge for radar systems, with traditional "stove-piped" spectrum allocations inadequately supporting the numerous competing demands for greater bandwidth [1-5]. Indeed, the position of the US DoD Chief Information Officer is "spectrum sharing is the way ahead to maintain economic dominance" [6]. Consequently, radar spectrum sharing techniques are necessary to preserve acceptable performance amidst the proliferation of other active RF users. Of course, depending on the particular manner of spectrum sharing, potential pitfalls may exist [7].

Cognitive radar (sometimes referred to as fully adaptive radar) attempts to improve performance and efficiency by "learning" from *a priori* observations to supplement decision making from low-level (e.g., waveform selection/design) up to high-level tasks (e.g., mission-level command and control) [5]. The most common forms of cognitive radar in the literature include optimization/selection of transmit parameters, waveforms, or filters [8-18]). In [8-10], a real-time transmit parameter optimization framework was implemented on the Ohio State CREW radar testbed via online optimization. Meanwhile, in [12–15] the Army Research Laboratory (in collaboration with multiple universities) implemented a real-time waveform spectral avoidance and notching method. Both real-time approaches leveraged Ettus x310 software-defined radios, providing the hardware foundation to implement cognitive systems due to their flexibility, low-cost, and shortened development times compared to legacy radar systems.

Growing RF congestion represents a transition from the era of noise-limited legacy radar to pervasive interference-limited operation. When in-band RF interference (RFI) is dynamically changing during the radar's coherent processing interval (CPI), one way this condition can be addressed (to a point) is by enabling the radar to become similarly dynamic. For instance, [14, 15] experimentally demonstrated real-time spectrum sensing and reactive notched waveform generation for per-pulse RFI mitigation.

Achieving real-time reactivity on a practical time scale can make optimal solutions impractical, though the evaluation of optimality (for a given metric [19]) is still beneficial to determine bounds on performance. Specifically, in [20] a heuristic method was introduced that mitigates correlation sidelobes arising from waveform spectral nulls. That method attempted to reduce sidelobes by tapering spectral null borders, and thereby soften sharp transitions, within the context of the particular random FM (RFM) waveform [21] subclass denoted as pseudorandom optimized FM (PRO-FM). While PRO-FM does involve optimization (via alternating time/frequency projections) the computational cost is low and therefore realizable in real-time [15]. However, the heuristic approach in [20] does not guarantee optimality.

Here, PRO-FM is likewise used, but in conjunction with the optimum LS null-constrained power spectrum to enforce low range sidelobe levels (based on matched filtering). The sidelobe level is then further reduced using LS mismatched filtering that was previously shown to be effective while maintaining spectral notches [22]. Since both the waveforms and mismatched filter are shaped according to the LS optimal power spectrum, their combination improves sidelobe performance with only rather modest mismatch loss.

II. Globally Optimum Sidelobe Reduction Bounds For Null-Constrained Power Spectra

To gain insight about the behavior of spectrally notched power spectra when attempting to minimize correlation sidelobes, it is interesting to first examine solutions to a well-posed (less constrained) objective statement. The power spectral density (PSD) and autocorrelation are a Fourier transform pair; therefore, waveforms designed to conform to a PSD template can be directly optimized for both autocorrelation and spectral properties. Moreover, doing so while constraining spectral null locations provides global minimum boundaries for waveform/filter spectral notches due to convexity.

This work was supported by the Office of Naval Research under Contract #N00014-20-C-1006. DISTRIBUTION STATEMENT A. Approved for Public Release.

Consider the optimization problem to design the PSD template, which can be written as

$$\begin{aligned} \min_{\mathbf{g}} \ & \|\mathbf{e} - \mathbf{A}^H\mathbf{g}\|_2^2 \\ \text{s.t.} \ & g_m \le \gamma_m \quad \text{for } m \in \Omega \\ & 0 \le g_m \quad \text{for } m = 0,1,\dots M-1 \end{aligned} \tag{1}$$

where $\mathbf{g}$ is the $M \times 1$ discretized PSD template with g_m as the mth element, $\mathbf{A}^H$ is an $M \times M$ inverse discrete Fourier transform (IDFT) matrix, $\mathbf{e}$ is the desired autocorrelation response, $(\cdot)^*$ denotes complex conjugation, $\|\cdot\|_2$ is the 2-norm operator, and γ_m is the constrained maximum value for the associated g_m and for m in the subset Ω (i.e. null constraints). Each element of $\mathbf{g}$ must be non-negative by definition of the PSD. The objective function in (1) therefore determines $\mathbf{g}$ such that the corresponding autocorrelation (via IDFT) has a minimized integrated sidelobe level (ISL), subject to spectral null constraints.

The problem formulation in (1) is a hybrid of non-negative LS and boxed LS, each being convex and having unique global solutions if $\mathbf{A}^H$ has full column rank (true for the DFT matrix) [23]. Different degrees of beamspoiling [24] can be achieved by replacing $\bar{M}$ rows of $\mathbf{A}^H$ (corresponding to autocorrelation mainlobe roll-off) with zeros, thus permitting different mainlobe widths and achievable sidelobe levels. The resulting beam-spoiled matrix still maintains full column rank; therefore, (1) is still convex and yields the globally optimal solution for $\mathbf{g}$.

For convenience, (1) is solved using the Matlab Constrained Optimization Toolkit [25] "fmincon". The resulting optimal PSDs for minimizing ISL, and their associated autocorrelation structures with various degrees of beamspoiling, are shown in Fig. 1. The spectral window length is chosen to be $M = 200$ samples. Notches are imposed at the band edges for containment, and an additional notch is imposed off-center. For all illustrated cases, each notch occupies 10% of the band with an enforced relative depth of 40 dB. The mainlobe resolution is defined by the ratio (%) of beamspoiled rows in $\mathbf{A}^H$ relative to the total spectral window length M.

A notable characteristic of the power spectra in Fig. 1 is that the larger primary band (between digital frequencies –0.1 and +0.4) maintains a majority of the power, with the smaller supplementary band (between digital frequencies –0.4 and –0.2) used to improve resolution. In fact, for the 6% beamspoiling case, the supplementary band is hardly occupied, implying that a sense-and-avoid [12] approach may be suitable depending on the desired resolution and sidelobe levels. Prior findings [26] that spectral notching near the band center degrades the achievable range sidelobe level is also confirmed in Fig 2. Compared to traditional windowing methods [27], the least squares optimal spectral templates are rather custom-designed via (1) to include spectral notches based on a prior spectrum-sensing process.

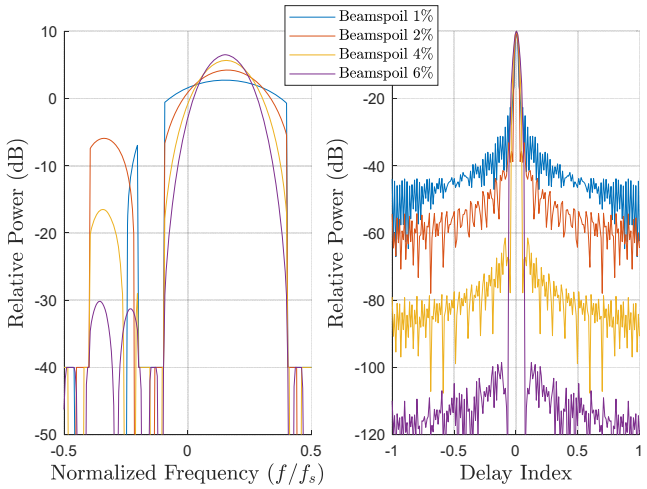

Fig. 1: Optimum ISL result for 40 dB spectral null and varied beamspoiling ratios of 1%, 2%, 4%, 6% relative to total window length

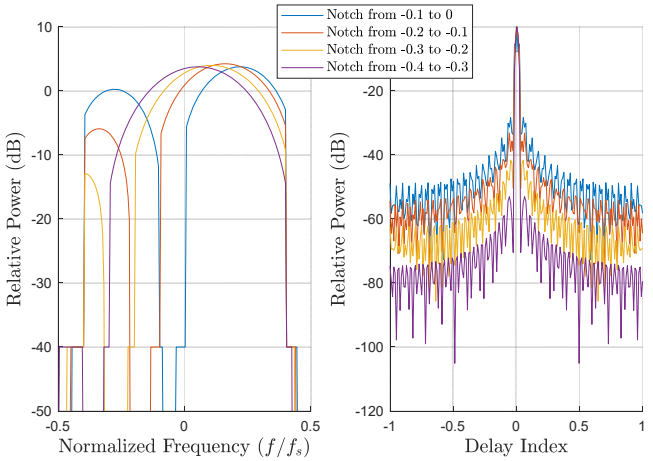

Fig. 2: Optimum ISL result for 40 dB spectral null and beamspoiling ratio of 2% relative to total window length, for different notch locations.

The cost function in (1) can be readily generalized to a p-norm framework

$$\begin{aligned} \min_{\mathbf{g}} \ & \|\mathbf{e} - \mathbf{A}^H\mathbf{g}\|_p^p \\ \text{s.t.} \ & g_m \le \gamma_m \quad \text{for } m \in \Omega \\ & 0 \le g_m \quad \text{for } m = 0,1,\dots M-1 \end{aligned} \tag{2}$$

with sufficiently large p well-approximating the peak sidelobe level (PSL) metric. The p-norm version still maintains convexity, so therefore global optimality is likewise preserved. The gradient of (2) is

$$\begin{aligned} \nabla_{\mathbf{g}} & \|\mathbf{e} - \mathbf{A}^H\mathbf{g}\|_p^p \\ & = -p\,\Re\{\mathbf{A}(|\mathbf{e} - \mathbf{A}^H\mathbf{g}|^{p-2} \odot (\mathbf{e} - \mathbf{A}^H\mathbf{g}))\}, \end{aligned} \tag{3}$$

where $\Re(\cdot)$ extracts the real part of the argument. For example, the resulting optimal PSDs and their corresponding autocorrelations for various degrees of beamspoiling are shown in Fig. 3 for $p = 8$. The same constraints are enforced as in Fig. 1 for the ISL case. Interestingly, these PSDs exhibit ridged structures when insufficiently beamspoiled. Similar to the ISL case, as the degree of beamspoiling is increased (relaxing autocorrelation mainlobe width) the sidelobe floor is

correspondingly reduced. This interplay between sidelobe level and mainlobe resolution is a fundamental trade-space for this design. A given degree of beamspoiling is necessary to achieve a desired dynamic range (i.e. sidelobe level); though increasing the beamspoiling factor does reduce 3-dB bandwidth and therefore degrades mainlobe resolution.

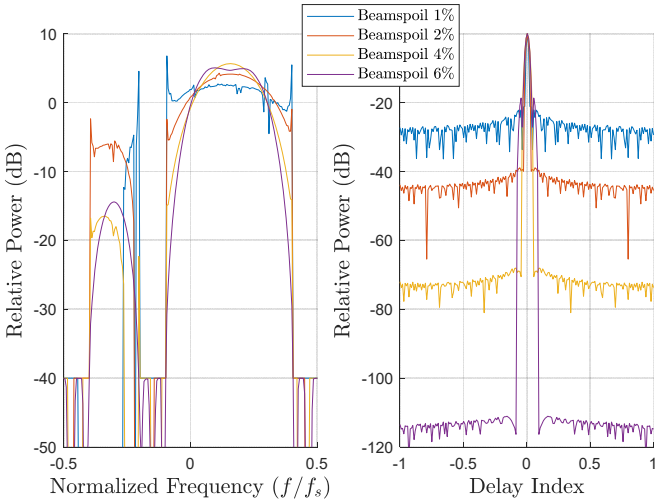

Fig. 3: Optimum PSL result ($p = 8$), for 40 dB spectral null and varied beamspoiling ratios of 1%, 2%, 4%, 6% relative to total window length

III. Spectrally-Notched RFM Waveform Design

Random FM (RFM) waveforms [21] provide design freedom and flexibility (due to non-repetition) while their FM structure ensures compatibility with high-power transmitters. Spectral notching algorithms [28-30] have been experimentally demonstrated to produce physically realizable RFM waveforms with >50 dB notch depths. Moreover, the low computational cost of spectral notching via zero-order reconstruction of waveforms (ZOROW) [30] enables real-time sense-and-notch (SAN) radar on an FPGA platform [14, 15].

The PRO-FM version of RFM [20] involves an alternating projections process to successively match a desired spectral template and a constant amplitude pulse of finite duration. Let T be the pulse width, B the 3-dB bandwidth, and f_s a sample rate that establishes the granularity of discretization (generally some factor greater than B to capture spectral roll-off). Denote $\mathbf{s}$ as the length-N digital representation of the desired analog waveform $s(t)$ discretized according to sample rate f_s that is to be designed to conform to desired PSD template $\mathbf{g}$. The kth iteration of the PRO-FM optimization alternates between enforcing the desired spectral template via

$$\tilde{\mathbf{s}}^{(k)} = \tilde{\mathbf{A}}^H \left\{ \mathbf{g}^{1/2} \odot \exp\left(j \angle \tilde{\mathbf{A}} \left\{ \mathbf{s}^{(k-1)} \right\} \right) \right\} \tag{4}$$

and enforcing the pulse envelope as

$$\mathbf{s}^{(k)} = \mathbf{u} \odot \exp\left(j \angle \tilde{\mathbf{s}}^{(k)} \right), \tag{5}$$

where $\tilde{\mathbf{A}}$ is the $M \times N$ truncated DFT matrix with $M \geq 2N-1$, $\tilde{\mathbf{A}}^H$ is the $N \times M$ truncated IDFT matrix, $\angle(\bullet)$ extracts the phase of the argument, and $\odot$ is the Hadamard product. Note that the square-root of the PSD in (4) is the magnitude spectrum of the signal. The length-N vector $\mathbf{u}$ is a discretization of rectangular pulse envelope $u(t)$ having duration T.

We compare the PRO-FM waveform spectra using two different desired templates $\mathbf{g}$, both intended to reduce sidelobes in the context of spectral nulls. The desired templates are the optimal PSD template discussed above and the ad hoc tapering method described in [20], where the latter was shown to be an effective (though suboptimal) solution. For this comparison, both templates have the same nulled region(s) defined by Ω, with the optimal template based on the constrained LS framework from Sect. II and the ad hoc template adhering to a notched Gaussian shape (same as [20]).

After PRO-FM optimization, the nulls of either spectrum may not achieve an acceptable depth; therefore, subsequent application of the ZOROW algorithm reinforces spectral notching while maintaining constant amplitude. The ZOROW algorithm operates on the phase values of the converged waveform, where the nth discretized element is

$$[\mathbf{s}]_n = e^{j\phi_n}, \tag{6}$$

which has associated phase values ϕ_n. This representation conforms to the analytical zero-order hold model used in digital-to-analog conversion. Collecting the phases into vector

$$\boldsymbol{\phi} = [\, \phi_1 \;\; \phi_2 \;\; \cdots \;\; \phi_N \,]^T, \tag{7}$$

the spectral representation of $\mathbf{s}$ takes the form [30]

$$S(f_m, \boldsymbol{\phi}) = \frac{\sin(\pi f_m T_s)}{\pi f_m} \sum_{n=1}^{N} \exp\left(-j(2\pi f_m (n-1/2) T_s + \phi_n) \right), \tag{8}$$

where $f_m = m\Delta f$ for integer $-\infty < m < \infty$ and $\Delta f \leq 1/(2T)$. The ZOROW formulation then employs cost function

$$\min_{\boldsymbol{\phi}} \sum_m |\, S(f_m; \boldsymbol{\phi}) \,|^2 \quad \text{for } m \in \Omega \tag{9}$$

in which the summation corresponds to frequency interval(s) from Ω for which notching is required and L iterations of the method in [30] are applied to deepen the nulled region(s).

IV. Application of Optimal Template for Spectral Shaping

Consider the case where 1000 waveforms are generated using the method above for both the optimal PSD template and the ad hoc template from [20]. The PRO-FM and ZOROW algorithms were implemented for $K = 200$ and $L = 1000$ iterations, respectively, to ensure full convergence. The number of waveform parameters $N = 200$ is held constant. The spectrum template size is set to $M = 4N - 1$. Spectral nulls for both templates are placed at both band edges and at a single off-center location, with each null occupying a normalized spectral width of $0.1 f_s$ (so $0.3 f_s$ in total).

For the ad hoc spectral template, $\mathbf{g}$ has a Gaussian shape with normalized 3-dB bandwidth $B = 0.5 f_s$, which imposes low range sidelobes before spectral notches are inserted. The additional tapering of sharp nulls takes the form of a raised-cosine function spanning $f_s/16$ at each null transition (one at each band edge and one either side of the off-center null, totaling four and spanning $0.25 f_s$).

The resulting average power spectrum and average autocorrelation responses over all 1000 waveforms for the ad-hoc case are shown in Fig. 4. The optimum PSD template (with beamspoiling ratio of 2%) is included for reference. While the ad hoc spectral template is clearly different from the optimal template (top panel), it does provide a reasonable approximation, with the resulting mean PSD response from the waveforms yielding a good match to the heuristic design. The coherently averaged (CA) autocorrelation computed over the waveform set (bottom panel) demonstrates the expected incoherent sidelobe averaging reduction [31] due to the non-repeating nature of RFM waveforms. While approaching the optimum, the ad hoc autocorrelation response does experience some mainlobe broadening and "shoulder" lobes.

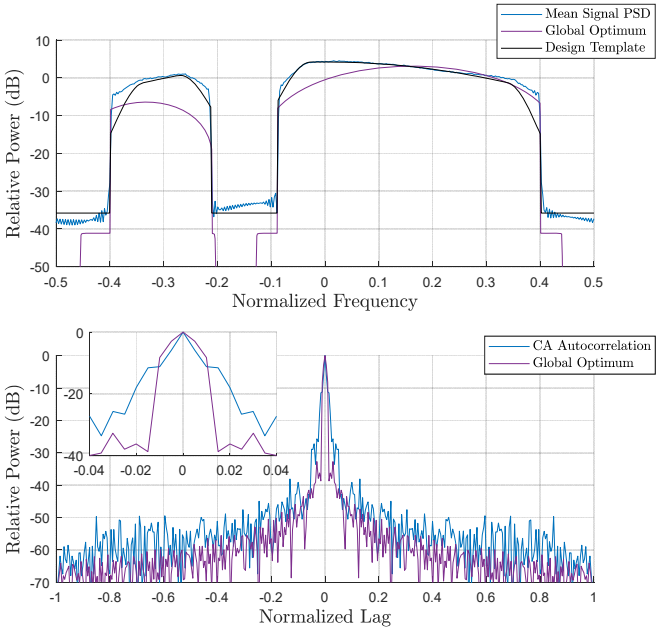

Fig. 4: Notched PRO-FM average PSD and coherently averaged autocorrelation from applying an **ad-hoc tapered [20]** spectral template

Now consider waveform design using the optimal template as shown in Fig. 5, which is based on the 2-norm version from (1). Clearly the mean PSD across the waveform set is closer to optimality than in the ad hoc case, and likewise for the ensuing CA autocorrelation. Of course, some deviation is also observed because perfect time-limited waveform spectrum shaping is not possible. Consequently, shoulder lobes are noticeably lower, yet are still present. However, the mainlobe broadening is essentially avoided. The sidelobe response is modestly lower than in the ad hoc case, though neither reach the optimal sidelobe roll-off.

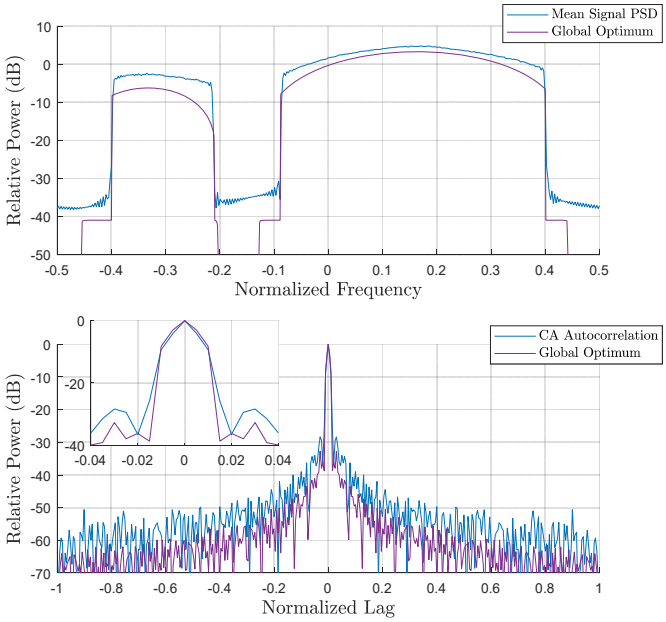

Fig. 5: Notched PRO-FM average PSD and coherently averaged autocorrelation from applying the **least-squares optimal** spectral template

V. Application of LS Mismatched Filtering

Because the optimum spectral template is based on LS in a 2-norm sense, it is logical to apply the LS mismatched filter (MMF) to these same waveform sets. The regularized LS-MMF of dimension $P \times 1$ is determined in closed form as [24, 32]

$$\mathbf{w}_{\mathrm{LS}} = \left(\mathbf{S}^H\mathbf{S} + \sigma\mathbf{I}\right)^{-1}\left(\mathbf{S}^H\mathbf{e}\right), \tag{10}$$

where σ is a diagonal loading factor, $\mathbf{I}$ is a $P \times P$ identity matrix, $\mathbf{e}$ is a length $N+P-1$ vector describing the desired correlation response, and $(\bullet)^H$ is the Hermitian operator. Convolution is represented by the $(N+P-1) \times P$ banded Toeplitz matrix

$$\mathbf{S} = \begin{bmatrix} s_1 & 0 & \cdots & 0 \\ \vdots & s_1 & \ddots & \vdots \\ s_N & \vdots & \ddots & 0 \\ 0 & s_N & & s_1 \\ \vdots & & \ddots & \vdots \\ 0 & \cdots & 0 & s_N \end{bmatrix}. \tag{11}$$

Here the desired correlation response is the IDFT of the desired spectrum $\mathbf{e} = \mathbf{A}^H\mathbf{g}$, such that $\mathbf{g}$ has dimension $M = N+P-1$ via (1) and P is set to $3N$. The term σ is set to 1% of the maximum eigenvalue of $\mathbf{S}^H\mathbf{S}$ to bias the MMF towards reducing spectral notch degradation (see [19]).

For the ad hoc case, Fig. 6 depicts the individual signal and filter PSDs, their cross-PSD, and the optimum PSD. The MMF elicits an average mismatch loss of 2.59 dB, but the signal/filter combination also almost perfectly overlaps with the optimal response. Consequently, the sidelobes likewise reach nearly to the optimum level. It also mitigates the notch degradation observed in [19].

Fig. 7 then shows the optimal template case, where we see the filter and cross-PSDs now align well with the optimal PSD and the mismatch loss is now 1.37 dB, a 1.22 dB improvement

over the ad hoc case. Of course, mismatch loss for both could be reduced by increasing the diagonal loading σ, though doing so will increase deviation from the optimal sidelobe level.

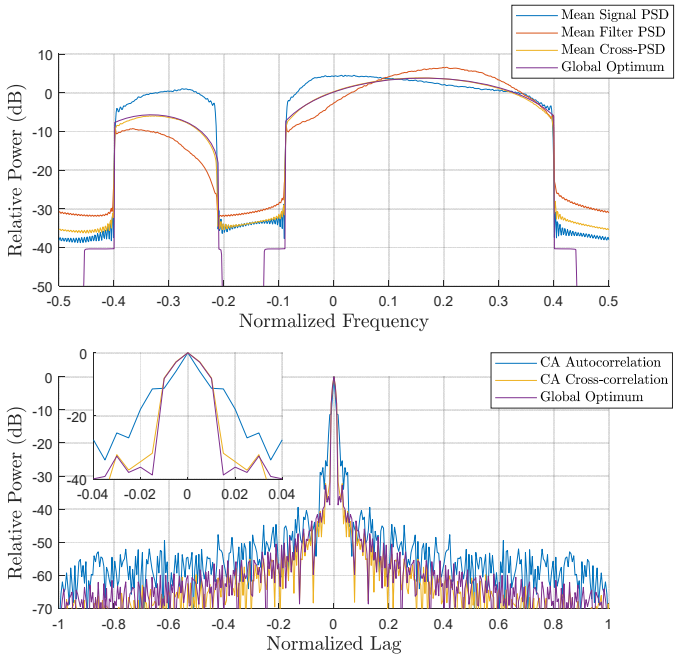

Fig. 6: Notched PRO-FM average PSD and coherently averaged autocorrelation from applying an **ad-hoc tapered** [20] spectral template. The individual signal and MMF responses are shown along with their combination (cross) and the optimum. While the former two (blue and red traces) appear to be almost complementary, the latter two (yellow and purple traces) achieve almost perfect overlap.

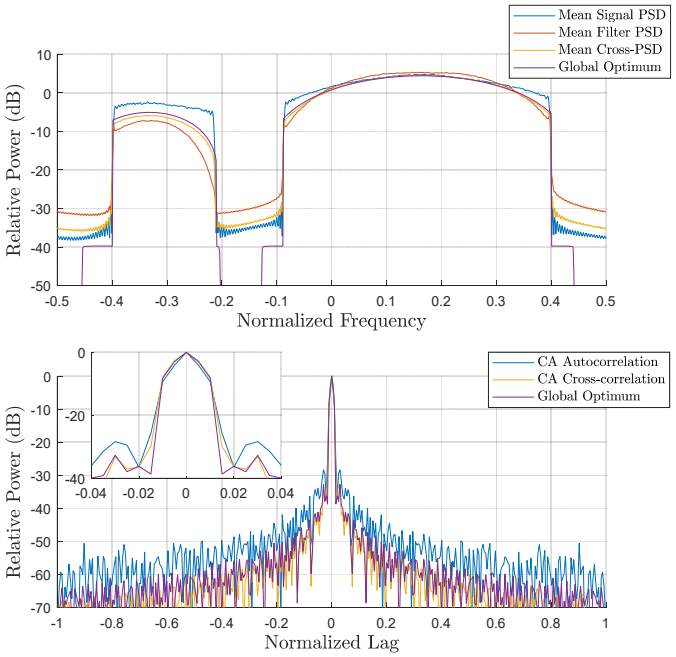

Fig. 7: Notched PRO-FM average PSD and coherently averaged autocorrelation from applying the **LS optimal** spectral template. The MMF and combination (cross) are now both close to the optimum (purple), with the signal+MMF (yellow) nearly overlapping it.

VI. Conclusions

The globally optimum power spectrum for correlation sidelobe reduction has been determined when portions of the spectrum are null constrained. By designing waveforms so that their spectrum closely matches the optimum, their attendant sidelobes likewise approach the optimum level. Application of the least-squares mismatched filter then closes much of the remaining sidelobe difference with mismatch loss in trade. Importantly, it is found that a previous ad hoc approach involving simple tapering of notch edges achieves near-optimal performance with a computational cost that is low enough for real-time implementation.

References

[1] H. Griffiths, *et al*, "Radar spectrum engineering and management: technical and regulatory Issues," *Proc. IEEE*, vol. 103, no. 1, pp. 85-102, Jan. 2015.

[2] J.M. Peha, "Sharing spectrum through spectrum policy reform and cognitive radio," *Proc. IEEE*, vol. 97, no. 4, pp. 708-719, Apr. 2009.

[3] M. Labib, V. Marojevic, A.F. Martone, J.H. Reed, A.I. Zaghloul, "Coexistence between communications and radar systems – a survey," *URSI Radio Science Bulletin*, vol. 2017, no. 362, pp. 74-82, Sept. 2017.

[4] M. López-Benítez, "Sensing-based spectrum awareness in cognitive radio: challenges and open research problems," *Intl. Symp. Communication Systems, Networks & DSP*, Manchester, UK, July 2014.

[5] S.Z. Gurbuz, H.D. Griffiths, A. Charlish, M. Rangaswamy, M.S. Greco, K. Bell, "An overview of cognitive radar: past, present, and future," *IEEE Aerospace & Electronic Systems Mag.*, vol. 34, no. 12, pp. 6-18, Dec. 2019.

[6] https://www.defense.gov/News/News-Stories/Article/Article/3165774/spectrum-sharing-is-way-ahead-to-maintain-economic-dominance-defense-official-s/

[7] M. Greenspan, "Potential pitfalls of cognitive radars," *IEEE Radar Conf.*, Cincinnati, OH, May 2014.

[8] G.E. Smith *et al*., "Experiments with cognitive radar," *IEEE Aerospace & Electronic Systems Mag.*, vol. 31, no. 12, pp. 34-46, Dec. 2016.

[9] A.E. Mitchell, J.L. Garry, A.J. Duly, G.E. Smith, K.L. Bell, M. Rangaswamy, "Fully adaptive radar for variable resolution imaging," *IEEE Trans. Geoscience & Remote Sensing*, vol. 57, no. 12, pp. 9810-9819, Dec. 2019.

[10] J.M. Christiansen, G.E. Smith, "Development and calibration of a low-cost radar testbed based on the universal software radio peripheral," *IEEE Aerospace & Electronic Systems Mag.*, vol. 34, no. 12, pp. 50-60, Dec. 2019.

[11] B. Ravenscroft, J.W. Owen, J. Jakabosky, S.D. Blunt, A.F. Martone, K.D. Sherbondy, "Experimental demonstration and analysis of cognitive spectrum sensing and notching for radar," *IET Radar, Sonar & Navigation*, vol. 12, no. 12, pp. 1466-1475, Dec. 2018.

[12] B.H. Kirk, R.M. Narayanan, K.A. Gallagher, A.F. Martone, K.D. Sherbondy, "Avoidance of time-varying radio frequency interference with software-defined cognitive radar," *IEEE Trans. Aerospace & Electronic Systems*, vol. 55, no. 3, pp. 1090-1107, June 2019.

[13] B.H. Kirk, A.F. Martone, K.D. Sherbondy, R.M. Narayanan, "Performance analysis of pulse-agile SDRadar with hardware accelerated processing," *IEEE Intl. Radar Conf.*, Washington, DC, Apr. 2020.

[14] J.W. Owen, C.A. Mohr, B.H. Kirk, S.D. Blunt, A.F. Martone, K.D. Sherbondy, "Demonstration of real-time cognitive radar using spectrally-notched random FM waveforms," *IEEE Intl. Radar Conf.*, Washington, DC, Apr. 2020.

[15] J. Owen, C. Mohr, B. Ravenscroft, S. Blunt, B. Kirk, A. Martone, "Real-time experimental demonstration and evaluation of open-air sense-and-notch radar," *IEEE Radar Conf.*, New York City, NY, Mar. 2022.

[16] A. Aubry, V. Carotenuto, A. DeMaio, A. Farina, L. Pallotta, "Optimization theory-based radar waveform design for spectrally dense environments," *IEEE Aerospace & Electronic Systems Mag.*, vol. 31, no. 12, pp. 14-25, Dec. 2016.

[17] A. Aubry, V. Carotenuto, A. DeMaio, A. Farina, A. Izzo, R.S.L. Moriello, "Assessing power amplifier impairments and digital predistortion on radar waveforms for spectral coexistence," *IEEE Trans. Aerospace & Electronic Systems*, vol. 58, no. 1, pp. 635-650, Feb. 2022.

[18] J. Guerci, *Cognitive Radar: The Knowledge-Aided Fully Adaptive Approach*, 2nd ed., Artech House, 2020.

[19] A.E. Mitchell, G.E. Smith, K.L. Bell, A. Duly, M. Rangaswamy, "Fully adaptive radar cost function design," *IEEE Radar Conf.*, Oklahoma City, OK, Apr. 2018.

[20] J. Jakabosky, B. Ravenscroft, S. Blunt, A. Martone, "Gapped spectrum shaping for tandem-hopped radar/communications & cognitive sensing," *IEEE Radar Conf.*, Philadelphia, PA, May 2016.

[21] S. D. Blunt, *et al*., "Principles and applications of random FM radar waveform design," *IEEE Aerospace & Electronic Systems Mag.*, vol. 35, no. 10, pp. 20-28, Oct. 2020.

[22] B. Ravenscroft, J. Owen, S. Blunt, A. Martone, K. Sherbondy, "Optimal mismatched filtering to address clutter spread from intra-CPI variation of spectral notches", *IEEE Radar Conf.*, Boston, MA, Apr. 2019.

[23] J. Mead, R. Renaut, "Least squares problems with inequality constraints as quadratic constraints," *Linear Algebra & its Applications*, vol. 432, no. 8, pp. 1936-1949, Apr. 2010.

[24] D. Henke, P. McCormick, S. D. Blunt, T. Higgins, "Practical aspects of optimal mismatch filtering and adaptive pulse compression for FM waveforms," *IEEE Radar Conf.*, Washington, DC, May 2015.

[25] https://www.mathworks.com/help/optim/ug/fmincon.html

[26] B. Ravenscroft, S.D. Blunt, C. Allen, A. Martone, K. Sherbondy, "Analysis of spectral notching in FM noise radar using measured interference," *IET Intl. Conf. Radar Systems*, Belfast, UK, Oct. 2017.

[27] A.W. Doerry, "Catalog of window taper functions for sidelobe control," Sandia Technical Report SAND2017-4042, Apr. 2017.

[28] T. Higgins, T. Webster, A.K. Shackelford, "Mitigating interference via spatial and spectral nulling: open air experimental results," *IEEE Radar Conf.*, Ottawa, Canada, Apr./May 2013.

[29] C.A. Mohr, S.D. Blunt, "Analytical spectrum representation for physical waveform optimization requiring extreme fidelity," *IEEE Radar Conf.*, Boston, MA, Apr. 2019.

[30] C.A. Mohr, J.W. Owen, S.D. Blunt, C.T. Allen, "Zero-order reconstruction optimization of waveforms (ZOROW) for modest DAC rates," *IEEE Intl. Radar Conf.*, Washington, DC, Apr. 2020.

[31] S.D. Blunt, E.L. Mokole, "Overview of radar waveform diversity," *IEEE Aerospace & Electronic Systems Mag.*, vol. 31, no. 11, pp. 2-42, Nov. 2016.

[32] M. H. Ackroyd and F. Ghani, "Optimum Mismatched Filters for Sidelobe Suppression," in *IEEE Transactions on Aerospace and Electronic Systems*, vol. AES-9, no. 2, pp. 214-218, March 1973.